Giant Electrothermal Conductivity and Spin-Phonon Coupling in an Antiferromagnetic Oxide

C. Chiorescu,[1] J. J. Neumeier,[2] and J. L. Cohn[1]
[1]Department of Physics, University of Miami, Coral Gables, Florida 33124, USA
[2]Department of Physics, Montana State University, Bozeman, Montana 59717, USA
(Received 6 June 2008; published 19 December 2008)

The application of weak electric fields ($\lesssim$100 V/cm) is found to dramatically enhance the lattice thermal conductivity of the antiferromagnetic insulator $CaMnO_3$ over a broad range of temperature about the Néel ordering point (125 K). The effect is coincident with field-induced detrapping of bound electrons, suggesting that phonon scattering associated with short- and long-ranged antiferromagnetic order is suppressed in the presence of the mobilized charge. This interplay between bound charge and spin-phonon coupling might allow for the reversible control of spin fluctuations using weak external fields.

DOI: 10.1103/PhysRevLett.101.257202 PACS numbers: 75.47.Lx, 66.70.−f, 75.80.+q, 71.55.−i

The strong magnetoelastic coupling present in certain antiferromagnetic (AFM) ferroelectrics [1] (e.g., hexagonal $YMnO_3$) has attracted considerable attention recently because of its importance in mediating a coupling between magnetic and electric orders [2] and the potential of such multiferroics for applications [3]. The hexagonal manganites also possess very strong spin fluctuations characteristic of a spin liquid well above their Néel temperatures, possibly related to geometric spin frustration. This raises the prospect of manipulating *dynamic* magnetoelastic coupling in the paramagnetic phase (PM) of these or other compounds using external fields.

Dramatic signatures of such coupling in $YMnO_3$ are a suppressed thermal conductivity [4] (κ) and anomalous ultrasonic attenuation [5] over a broad temperature range in the PM phase. Two AFM oxides with quite similar features in their thermal conductivities are the transition-metal monoxide, MnO [6] ($T_N = 118$ K), and orthorhombic $CaMnO_3$ [7,8] ($T_N \sim 125$ K). Like $YMnO_3$, both of these materials possess large exchange striction [9,10] (with changes in lattice constants at $T < T_N$, $\Delta a/a \gtrsim 10^{-4}$), significant spin frustration [11,12] $\Theta/T_N \sim 4$–5 (Θ is the Curie-Weiss temperature), and strong short-range spin correlations extending well above T_N [11,13]. The suppressed thermal conductivities in the PM phase of $YMnO_3$ and $CaMnO_3$ (and by extension, MnO) have been proposed to arise from the scattering of acoustic phonons by nanoscale strains generated by short-ranged spin correlations [4,7]. This scattering diminishes rapidly when long-range order is established, giving rise to sharp increases in κ at $T < T_N$.

$CaMnO_3$ is distinguished from $YMnO_3$ and MnO by the presence of low-lying electron donor levels (oxygen vacancies) from which a small density of mobile electrons ($\Delta n \sim 10^{16}$ cm^{-3}) can be released under relatively weak applied electric fields ($F \lesssim 100$ V/cm) [14]. Here we demonstrate that these mobilized carriers are associated with a substantial reduction in phonon scattering, yielding relative changes in κ with field, $(1/\kappa)(\Delta\kappa/\Delta F)$ that are 2 orders of magnitude larger than found in quantum paraelectrics such as $KTaO_3$ and $SrTiO_3$ [15] where the field couples to soft-mode phonons. The apparent absence of permanent electric dipoles or lattice anomalies in $CaMnO_3$ leads to the hypothesis that the mobilized electrons themselves mediate a suppression of phonon scattering from strain induced by short- and long-ranged magnetic order.

Measurements were performed on single-crystal and polycrystalline specimens of $CaMnO_3$. Their preparation methods and physical properties have been reported elsewhere [8,14,16–18]. We focus here on the crystal (dimensions $2 \times 0.9 \times 0.05$ mm^3) for which κ was measured for two different oxygen configurations produced by annealing at 600 °C in flowing oxygen and air, respectively. The net carrier density for the oxygen-annealed state, as determined from room-temperature Hall measurements [14], was $N \simeq 6 \times 10^{18}$ cm^{-3}. This corresponds to $\sim 3 \times 10^{-4}$ electrons per formula unit, attributed to a very small oxygen deficiency. The carrier density after annealing in air is estimated [18] from the increase in room-temperature thermopower (-530 μV/K to -370 μV/K) to be $N \simeq 4 \times 10^{19}$ cm^{-3}. κ was measured with a steady-state technique employing a heater and 25 μm-diameter chromel-constantan thermocouple; four-probe electrical resistivity (ρ) was measured during the same experiments. $\kappa(I, T)$ was measured for the air-annealed crystal in the presence of dc transport currents ($I = 5$ nA–10 mA). With the specimen suspended in vacuum and thermally anchored at only one end, Joule heating was significant at the highest currents. The average specimen temperature (relative to a resistance sensor mounted on the cold stage) was monitored with a second thermocouple following application of a transport current, and allowed to stabilize prior to energizing the specimen heater for determining κ. Linearity in the heater power-ΔT response was confirmed at various temperatures throughout the measurement range.

Figure 1 (lower panel) shows $\kappa(T)$ after oxygen (dashed curve) and air (circles) annealing. The $I = 0$ and $I = 10$ mA plots for air annealing are labeled. Constant electric

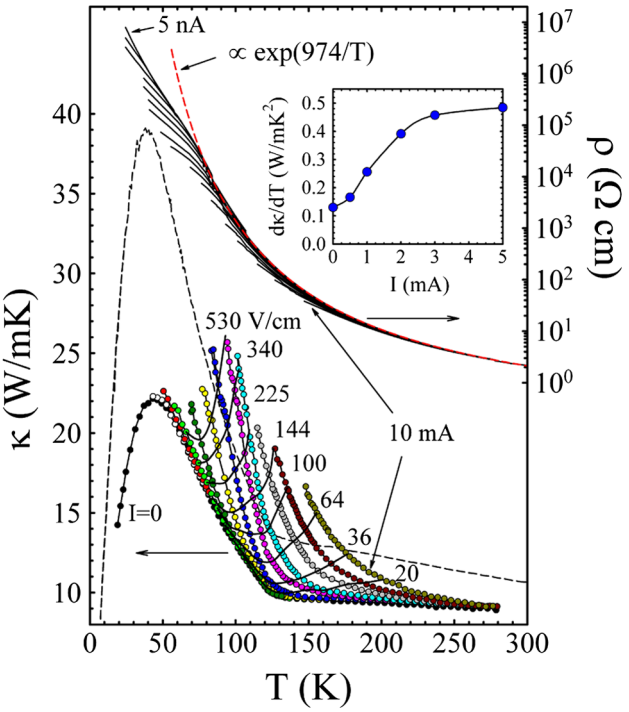

FIG. 1 (color online). Lower panel (left ordinate): $\kappa(T)$ for the air-annealed $CaMnO_3$ crystal (circles) at various transport currents, from right to left (in mA): 10, 5, 3, 2, 1, 0.5, 0.25, 0.1, 0.05, 0.01, 0. The solid curves bridging $\kappa(T)$ plots are contours of constant electric field (values labeled). The dashed curve represents data for the oxygen-annealed crystal for $I = 0$. Upper panel (right ordinate): $\rho(T)$ for the same currents as $\kappa(T)$ as well as the following (in μA): 5, 3, 1, 0.3, 0.1, 0.03, 0.01, 0.005. Inset: current dependence of the slope, $d\kappa/dT$, for air annealing.

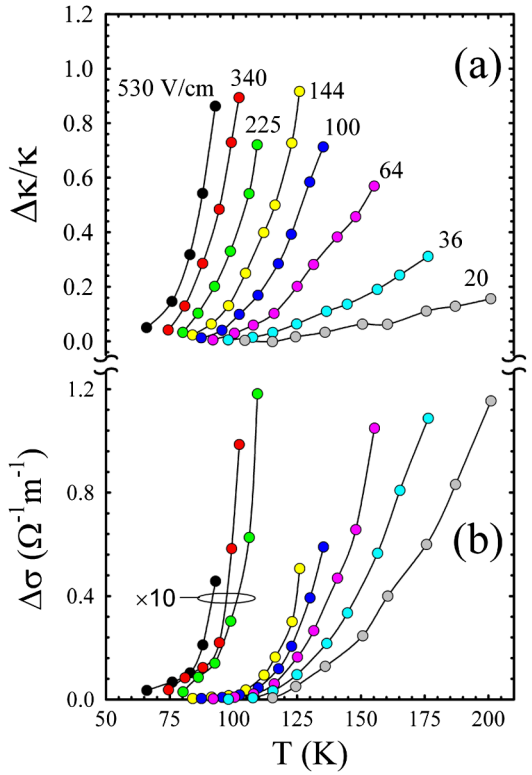

FIG. 2 (color online). (a) Fractional change in thermal conductivity vs temperature at constant electric fields, (b) Field-induced change in electrical conductivity for the same field values as in (a).

field (F) contours (with values labeled) are represented by solid curves bridging the constant current plots. These fields, $F = \rho J$, were determined from $\rho(T)$ data (upper panel). The abrupt upturn in κ upon entering the AFM ordered phase is evident near $T_N \approx 120$ K. Note that for the $I = 0$ curves the slope just below T_N, $d\kappa/dT|_{T_N}$, is greater for oxygen annealing, and increases with I for the air-annealed crystal (inset, Fig. 1). These features are discussed further below. The data were reproducible upon thermal and current cycling, and after subsequent reannealing.

Figure 2(a) shows the T dependence of the fractional change in thermal conductivity, $(\Delta\kappa/\kappa) \equiv [\kappa(F, T) - \kappa(0, T)]/\kappa(0, T)$, computed for these values of F. The enhancement of κ in field is substantial, approaching 100% for fields $F > 100$ V/cm in the range 80 K $< T <$ 130 K, and becomes negligible at lower temperatures. Qualitatively similar results were found for the polycrystalline specimen, with a temperature interval for the largest field effects lower by about 50 K.

The field-enhanced κ correlates with an increased electrical conductivity, $\Delta\sigma = \sigma(F, T) - \sigma(0, T)$ [Fig. 2(b)]. As demonstrated by prior Hall effect studies on this same crystal [14], the mechanism underlying the increase in σ is Poole-Frenkel [19] release of carriers from Coulomb traps (oxygen vacancy donor levels) via field-assisted barrier lowering. However, it is clear that the thermal conductivity of these mobilized electrons cannot account for the increase in κ. For example, $\Delta\sigma \sim 0.5\ \Omega^{-1}\,m^{-1}$ at $F =$ 144 V/cm and $T = 126$ K, corresponding to an increase in the electron density, $\Delta n \simeq 3 \times 10^{16}$ cm^{-3} (using a mobility [18] $\sim$1 cm^2/V s), about 50% of the equilibrium value at that temperature. The Wiedemann-Franz law, which provides an upper-bound estimate on the electronic thermal conductivity, yields $\Delta\kappa_e = L_0\Delta\sigma T \simeq 1.5 \times 10^{-6}$ W/mK, nearly 7 orders of magnitude smaller than observed. Spin-wave heat conduction, though a possible contributor to κ at low T in the ordered phase, cannot account for κ well above T_N. Thus the increase of κ must have its origin in reduced phonon scattering.

Bound electrons may cause phonon scattering through static local distortions of bond lengths [20] or more extended, dynamic polaronic distortions, and possibly the diminution of this scattering as electrons become mobile in field explains the observations. But this proposal must be viewed as implausible given that the fraction of bound electrons released is very small, $\sim\Delta n/N \lesssim 10^{-3}$, so that the density of such distortions is altered negligibly in field. Further supporting this view, κ at the highest F for the air-

annealed crystal exceeds that in zero field for the oxygen-annealed state (Fig. 1), in spite of the fact that the bound electron density in the former exceeds that of the latter by an order of magnitude. In addition, there is no evidence of permanent electric dipoles in this material [17,21], the alignment of which in weak fields might conceivably alter the phonon scattering. This leads us to consider that the *mobilized* electrons themselves mediate a suppression of phonon scattering.

In order to assess how this might occur and to gain insight into the origin of the strong PM-phase phonon scattering, it is instructive to examine changes in structure induced by the onset of magnetic order. Anomalous Mn motion, stabilized at $T < T_N$, was recently proposed to explain the κ behavior of hexagonal $YMnO_3$ [22]. However, the unusual Mn-O bond length changes [1] motivating this proposal are absent in the average and local structure of $CaMnO_3$ [23]. On the other hand, rotations of the MnO_6 octahedra couple strongly to the magnetic order in $CaMnO_3$ [13,23] and provide a mechanism through which spin fluctuations at $T > T_N$ may induce strain that scatters heat-carrying acoustic modes. Perturbations due to the polaronic motion [14,18,24] of mobilized electrons may compete with the distortions favored by short-ranged AFM ordered domains.

Consider the scenario for phonon scattering by spin fluctuations introduced by Sharma *et al.* [4]. Strain fields associated with short-ranged AFM spin-ordered regions have spatial extent given by the spin correlation length ξ. Slowly fluctuating on the time scale of lattice vibrations, they scatter acoustic phonons. For the case $\lambda_p \ll \xi$ (where λ_p is the phonon wavelength [25]), their scattering rate can be approximated (for a spherical spin-correlated domain) as $\tau_{\rm mag}^{-1} = p_0 v \pi (\xi/2)^2$ (p_0 and v are the density of scatterers and phonon velocity, respectively). This scattering should be sharply diminished at $T < T_N$ as long-range magnetic order is established. Residual strain in AFM domain walls and other defects (e.g., twins) likely scatter phonons to low temperatures as evidenced by a phonon mean-free path [26], $\ell_{\rm ph} = 3\kappa/Cv$, that remains <1 μm at the lowest measured T.

To examine this picture more quantitatively we employ the Debye-Calloway model [27] to compute the lattice thermal conductivity, adding $\tau_{\rm mag}^{-1}$ to a sum of traditional phonon scattering rates arising from other phonons (Umklapp), dislocations, and pointlike defects [28]. We restrict our analysis to the PM phase and for simplicity ignore possible temperature dependencies of p_0 and ξ, taking $\gamma \equiv p_0 \pi (\xi/2)^2$ as a constant parameter for $T > T_N$. The $I = 0$ data for air and oxygen annealing were first fitted by assuming the traditional phonon scattering terms to be independent of the annealing treatment, and the computed κ in the absence of magnetic scattering ($\gamma = 0$) was constrained to match the oxygen-annealed data at the lowest T and to exceed the highest measured values (including those for air annealing in applied field) at intermediate T. Subsequently, the data for air annealing in applied field were fitted with γ as the only adjustable parameter.

Figure 3 compares the calculated (solid curves) and measured $\kappa(T)$. Also shown is the hypothetical $\kappa(T)$ in the absence of magnetic scattering ($\gamma = 0$, dashed curve). The values of $\gamma = 2.51(0.82) \times 10^7$ m^{-1} for air (oxygen) annealing are similar to that employed for $YMnO_3$ [4]. For self-consistency, the distance between scatterers, $d = 2(3/4\pi p_0)^{1/3}$, must be larger than their size ξ. Both $YMnO_3$ [4] and MnO [11] have comparable values of $\xi \sim$ 20–50 Å. In the absence of a direct measurement of ξ for $CaMnO_3$, taking $\xi = 40$ Å implies a density of scatterers $p_0 = 2.0 \times 10^{18}$ cm^{-3} for air annealing, or equivalently, $d \simeq 100$ Å $> \xi$ as required.

Fitting the model to $\kappa(F)$ at fixed T yields the decrease in magnetic scattering vs the relative change in mobile carrier density (inset of Fig. 3). The decrease in γ, by up to a factor of 10 at the highest applied fields near T_N, implies a decrease in p_0, ξ or both.

The nucleation of AFM domains in the PM phase and their growth in the ordered phase likely depend on domain-wall pinning near lattice defects [29]. Mobilized electrons could reduce p_0 by depinning AFM domains, an idea motivated by comparing the zero-field data for air and oxygen annealing. The larger κ and $d\kappa/dT|_{T_N}$ observed for the more oxygenated crystal in the ordered phase (Fig. 1) suggest a coarsening of the domain structure, consistent with observations in $Gd_2(MoO_4)_3$ of strong phonon scattering at ferroelastic domain boundaries [30].

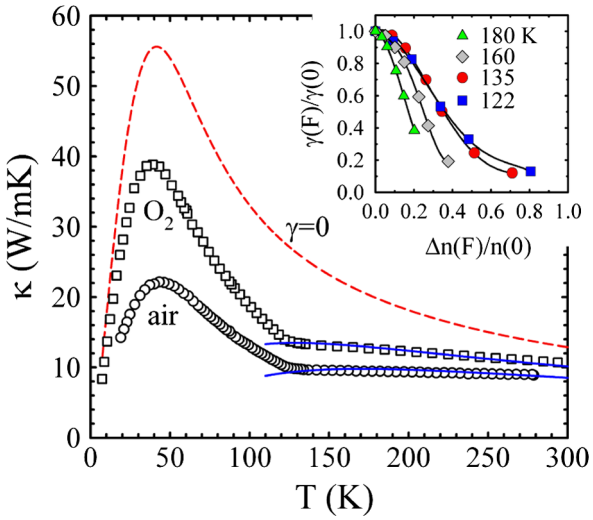

FIG. 3 (color online). Comparison of calculated (curves) and measured (symbols) $\kappa(T)$ for $I = 0$. The dashed curve is the computed κ in the absence of magnetic scattering ($\gamma = 0$). The solid curves used $\gamma = 2.51(0.82) \times 10^7$ m^{-1} for air (oxygen) annealing. Inset: magnetic scattering strength versus field-induced carrier density determined from fits to $\kappa(F)$ at fixed T.

Oxygen vacancies or their complexes are thus implicated in pinning (the estimate of p_0 above suggests that $\sim$10% of vacancies participate in pinning).

The correlation between κ and $d\kappa/dT|_{T_N}$ in applied electric field (Fig. 1) suggests that mobilized electrons cause depinning. The polaronic motion of charge carriers can increase the frequency of spin fluctuations [31], effectively reducing p_0. There is precedent for the diminution of ξ by light charge-carrier doping in $Ca_{1-x}La_xMnO_3$ [13] and $La_{2-x}Sr_xCuO_4$ [31]. However, the carrier densities in these cases are several orders of magnitude larger than Δn induced by field in the present experiments. Both κ and $d\kappa/dT|_{T_N}$ decrease with substitutional doping in $Ca_{1-x}La_xMnO_3$ [8], contrary to the field-induced trend, but this may simply reflect the predominance of additional scattering from substitutional disorder. More direct measurements of the AFM correlations in $CaMnO_3$ as functions of temperature and applied electric field are clearly called for to further test and refine the ideas put forward here.

In summary, the present measurements of thermal conductivity in $CaMnO_3$ imply that a small density of electrons released from donor states in weak electric fields substantially reduce the scattering of phonons associated with short- and long-ranged AFM order. The results suggest that the correlated spin volume in the PM phase is highly sensitive to the injected carrier density and reversibly controlled by a transport current. Strong AFM spin fluctuations, magnetostriction, and the presence of loosely bound charges in defect states appear to be key ingredients underlying the observations. This novel manipulation of dynamic magnetoelastic coupling motivates further studies of spin correlations in this compound or others having similar characteristics.

This material is based upon work supported by the National Science Foundation under Grants No. DMR-0072276 (Univ. Miami) and No. DMR-0504769 (Mont. St. Univ.), and the Research Corporation (Univ. Miami).

[1] S. Lee *et al.*, Nature (London) **451**, 805 (2008); J. Cao *et al.*, Phys. Rev. Lett. **100**, 177205 (2008); D. Meier *et al.*, New J. Phys. **9**, 100 (2007); F. Ye *et al.*, Phys. Rev. B **73**, 220404(R) (2006).

[2] W. Eerenstein, N. D. Mathur, and J. F. Scott, Nature (London) **442**, 759 (2006).

[3] M. Fiebig, J. Phys. D **38**, R123 (2005); T. Kimura *et al.*, Nature (London) **426**, 55 (2003); N. Hur *et al.*, *ibid.* **429**, 392 (2004); T. Lottermoser *et al.*, *ibid.* **430**, 541 (2004).

[4] P. A. Sharma *et al.*, Phys. Rev. Lett. **93**, 177202 (2004).

[5] M. Poirier *et al.*, Phys. Rev. B **76**, 174426 (2007).

[6] G. A. Slack and R. Newman, Phys. Rev. Lett. **1**, 359 (1958).

[7] J.-S. Zhou and J. B. Goodenough, Phys. Rev. B **66**, 052401 (2002).

[8] J. L. Cohn and J. J. Neumeier, Phys. Rev. B **66**, 100404(R) (2002).

[9] B. Morosin, Phys. Rev. B **1**, 236 (1970).

[10] Y. Moritomo *et al.*, Phys. Rev. B **64**, 214409 (2001).

[11] A. Renninger, S. C. Moss, and B. L. Averbach, Phys. Rev. **147**, 418 (1966); H. Betsuyaku, Solid State Commun. **26**, 345 (1978).

[12] J. J. Neumeier and D. H. Goodwin, J. Appl. Phys. **85**, 5591 (1999).

[13] E. Granado *et al.*, Phys. Rev. Lett. **86**, 5385 (2001).

[14] C. Chiorescu, J. L. Cohn, and J. J. Neumeier, Phys. Rev. B **76**, 020404(R) (2007).

[15] W. H. Huber, L. M. Hernandez, and A. M. Goldman, Phys. Rev. B **62**, 8588 (2000).

[16] J. J. Neumeier and J. L. Cohn, Phys. Rev. B **61**, 14 319 (2000).

[17] J. L. Cohn, M. Peterca, and J. J. Neumeier, Phys. Rev. B **70**, 214433 (2004).

[18] J. L. Cohn, C. Chiorescu, and J. J. Neumeier, Phys. Rev. B **72**, 024422 (2005); C. Chiorescu, J. J. Neumeier, and J. L. Cohn, *ibid.* **73**, 014406 (2006).

[19] J. Frenkel, Phys. Rev. **54**, 647 (1938).

[20] J. L. Cohn *et al.*, Phys. Rev. B **56**, R8495 (1997).

[21] A. Filippetti and N. A. Hill, Phys. Rev. B **65**, 195120 (2002).

[22] J.-S. Zhou *et al.*, Phys. Rev. B **74**, 014422 (2006).

[23] E. S. Bozin *et al.*, J. Phys. Chem. Solids **69**, 2146 (2008).

[24] Y. R. Chen and P. B. Allen, Phys. Rev. B **64**, 064401 (2001); H. Meskine, T. Saha-Dasgupta, and S. Satpathy, Phys. Rev. Lett. **92**, 056401 (2004); H. Meskine and S. Satpathy, J. Phys. Condens. Matter **17**, 1889 (2005).

[25] A resonable estimate for thermal phonons is $\lambda_p \sim h\upsilon/(3.8k_BT) \approx$ 2–6 Å in the PM phase.

[26] Specific heat (C) data for $CaMnO_3$ are reported by Y. Moritomo *et al.*, Phys. Rev. B **64**, 214409 (2001); A. Cornelius *et al.*, *ibid.* **68**, 014403 (2003). The sound velocity $\upsilon = 4800$ m/s employed represents an average computed from the experimental Debye temperature (Θ_D).

[27] R. Berman, *Thermal Conduction in Solids* (Clarendon, Oxford, 1976).

[28] The scattering of phonons of frequency $\omega = \upsilon q$ by other phonons (U processes), dislocations, and point defects were represented by rates $A_1\omega^2T\exp(-\Theta_D/bT)$, $A_2\omega$, $A_3\omega^4$. Boundary scattering was found to be negligible in the measured temperature range. Parameter values (the same for air and oxygen annealing) were $A_1 = 2.63 \times 10^{-18}$ s K^{-1}, $A_2 = 7.65 \times 10^{-5}$, and $A_3 = 2.36 \times 10^{-43}$ s^3. These values are comparable to those found for $YMnO_3$ (Ref. [4]). b was taken as 5 (Ref. [27]).

[29] Yin-Yuan Li, Phys. Rev. **101**, 1450 (1956); B. K. Tanner, Contemp. Phys. **20**, 187 (1979).

[30] S. Mielcarek *et al.*, Proceedings of the 11th IEEE International Symposium on Applications of Ferroelectrics, ISAF98 (1998), p. 415.

[31] V. Kataev *et al.*, J. Phys. Condens. Matter **11**, 6571 (1999); K. Hirota *et al.*, Physica (Amsterdam) **357–360C**, 61 (2001).